A multimodel-based screening framework for C-19 using deep learning-inspired data fusion.

SHANKAR, A., RIZWAN, P., MEKALA, M.S., ELYAN, E., GANDOMI, A.H., MAPLE, C. and RODRIGUES, J.J.P.C.

2024

A Multimodel-Based Screening Framework for C-19 Using Deep Learning-Inspired Data Fusion

Achyut Shankar, P Rizwan, M S Mekala, Eyad Elyan, Amir H. Gandomi, Carsten Maple, Joel J. P. C. Rodrigues

***Abstract*—In recent times, there has been a notable rise in the utilization of Internet of Medical Things (IoMT) frameworks particularly those based on edge computing, to enhance remote monitoring in healthcare applications. Most existing models in this field have been developed temperature screening methods using RCNN, face temperature encoder (FTE), and a combination of data from wearable sensors for predicting respiratory rate (RR) and monitoring blood pressure. These methods aim to facilitate remote screening and monitoring of Severe Acute Respiratory Syndrome Coronavirus (SARS-CoV) and COVID-19. However, these models require inadequate computing resources and are not suitable for lightweight environments. We propose a multimodal screening framework that leverages deep learning-inspired data fusion models to enhance screening results. A Variation Encoder (VEN) design proposes to measure skin temperature using Regions of Interest (RoI) identified by YoLo. Subsequently, the multi-data fusion model integrates electronic records features with data from wearable human sensors. To optimize computational efficiency, a data reduction mechanism is added to eliminate unnecessary features. Furthermore, we employ a contingent probability method to estimate distinct feature weights for each cluster, deepening our understanding of variations in thermal and sensory data to assess the prediction of abnormal COVID-19 instances. Simulation results using our lab dataset demonstrate a precision of 95.2%, surpassing state-of-the-art models due to the thoughtful design of the multimodal data-based feature fusion model, weight prediction factor, and feature selection model.**

***Index Terms*—Covid-19, Thermal imaging, Deep learning, Measurement index, Machine learning, IoMT, Thingspeck.**

I. Introduction

HUMAN body temperature and respiratory rate and blood pressure are well know indications of body health issues [1]. In particularly taking the consideration of covid-19 pandemic case-study, a fast and lightweight measurement models are essential for remote monitoring deceases like severe acute respiratory syndrome (SARS) and COVID-19. According to World Health Organisation (WHO) reports, approximately twenty-two million deaths worldwide due to C-19 disease as of August 2020 [2], [3]. Basically, when the immune system detects the presence of a pathogen (such as a virus or bacteria), it will signal the hypothalamus in the brain to raise the body's temperature. Therefore, detection of skin temperature has become an essential primary feature in this study and more specifically usage of thermal sensors [4]. Non-contact situations and performance limitations of digital thermometers, along with other smart devices for temperature screening, pose challenges in deploying them at public places. In this regard, we propose a technique that utilizes both thermal images and sensory data for effective screening and monitoring in crowded areas. The *Thermal image* visualizes the temperature variations of objects, with applications related to health care [5], [6], [7]. Assessing COVID-19 abnormal factors from medical reports is challenging because most medical records lack structure due to the large volume of data collected daily. So the alternate option is using wearable sensors for uninterrupted monitoring, but in some cases, these results might be inaccurate due to signal communication noise [8], [9], [10]. The regular symptoms range for fever 83-99%, cough 59-82%, fatigue 44-70%, loss of appetite 40-84%, short-breath from 31-40%. These symptoms can be assessed with human wearable sensors, but combining medical and sensor data for assessing specific task towards making reliable decisions is a challenging task. So, there is scope for designing an intelligent decision-making system that utilizes sensed data, medical data, and image data to forecast hidden features and characteristics in monitoring non-contact situations. Many existing models have focused on developing hybrid models that use weight factors to extract insightful information for assessing risk factors from informal data [11], but they have resulted in redundancies and false classifications. The recurring issue of repeated weights in each class affects prediction accuracy. In our model, we eliminate unimportant features by assigning specific weights to each class for more effective disease classification. We design an intelligent framework for detecting and monitoring C-19, combining a Deep Learning (DL) backbone with essential data fusion models. The data comprises statistical data from wearable sensors and thermal images from cameras. We assess the adaptive features of this combined data by applying

Achyut Shankar is with Secure Cyber Systems Research Group (SCSRG), WMG, University of Warwick, Coventry, CV74AL, UK, and University Centre for Research Development, Chandigarh University, Mohali, Punjab, 140413, India and Department of Computer Science and Engineering, Graphic Era Deemed to be University, Dehradun, 248002, India as well as School of Computer Science Engineering, Lovely Professional University, Phagwara,Punjab, 144411, India E-mail: ashankar2711@gmail.com

P Rizwan is with Decentralized Science Lab (DSL), College of Computing and Software Engineering, Kennesaw State University, 680 Arntson Drive, Marietta, 30060, USA, E-mail: prizwan5@gmail.com

M S Mekala, Eyad Elyan are with School of Computing, Robert Gordon University, AB10 7GE Aberdeen,U.K. (e-mail: ms.mekala@rgu.ac.uk and e.elyan@rgu.ac.uk

Amir H Gandomi is with Faculty of Engineering and Information Technology, University of Technology Sydney, Ultimo, NSW 2007, Australia (e-mail: gandomi@uts.edu.au), and University Research and Innovation Center (EKIK), Óbuda University, 1034 Budapest, Hungary

Carsten Maple is with Secure Cyber Systems Research Group (SCSRG), WMG, University of Warwick, Coventry, UK, E-mail: cm@warwick.ac.uk

Joel J. P. C. Rodrigues is with the College of Computer Science and Technology, China University of Petroleum (East China), Qingdao 266555, China, and Instituto de Telecomunica, 6201-001 Covilh, Portugal (e-mail: joeljr@ieee.org).

prognostic probability models to estimate the weight of the feature vectors. The main contributions of this paper are as follows:

1) Design a Variance Encoder (VE) to assess the disparities in Regions of Interest (ROIs) generated by YoLo for screening skin temperature and lip color. Enhance its functionality to track objects using abnormal ROIs in crowded environments.
2) Design an Information Attain (IA) model to reduce noise by eliminating unnecessary features to simplify the dataset. Additionally, design a Predictive Probability (PP) method to estimate the weight of features for each class to improve the success rate of predictions.
3) Develop a decision-making system using ThingSpeak with measurement indexing levels. This system triggers the actions based on evaluated information, and generates a diet strategy. The strategy is based on ontology-inspired Semantic Rule (OSR_i), which refers to a list of diet plan activities aimed at enhancing the immune system.

The rest of the paper is structured as follows: Section II presents a brief related work. Section III describes a proposed system framework and discusses the PP method, Variance Encoder (VE), the IA model, and an adaptive measurement index for the decision-making system. Section IV describes the experimental and simulation results. Finally, Section V summarises the conclusions and future studies.

II. Related Works

Most existing machine learning-based vision models successfully detect and predict COVID-19. Applications in references [12] and [13] utilize Internet of Things (IoT) and Internet of Medical Things (IoMT), assisting hospitals in enforcing remote monitoring. Recent articles, such as those referenced by [14], [15], [16], [17], [18], [19], employ machine learning, AI, and deep learning techniques for predicting COVID-19, which encompasses segmentation in X-rays and CT scans, with common models including ResNet-50, AlexNet, DenseNet, ResNet-101. Prevalent segmentation models such as U-Net, DeepLab, MiniSeg, and 3D U-Net are commonly utilized, while Faster R-CNN with VGG as the base network is employed for COVID detection [20], [21], [22]. The subsections below describe the feature extraction-based and thermal imaging models, respectively.

A. Feature identification models

Most studies have been developed to identify characteristics and the evaluation of disease features, particularly the evaluation of lung nodules and heart disease, primarily from a predictive perspective. In [23], a multisensory framework for data collection using fog/edge computing, combined with the random forest classification model, is utilized for heart disease identification. Meanwhile, in [24], a correlation system is employed to identify future relevant features, which are assessed based on data fusion. This approach achieved 98% accuracy with eight features but has not met the needs of affected patients. In [25], researchers proposed a fuzzy genetic algorithm to streamline medical uncertainty data. They utilized a Wavelet transformer to evaluate features and attempted to reduce computational workloads by eliminating unnecessary data fields. In [26], random and linear models were employed for disease prediction, achieving an accuracy of 88.5%. Fourier transformation in [27] has been used to estimate health-related diseases based on time constraints, and the results show that it effectively analyses diseases with combined data. In [3], IoT-cognitive radio (ICR) framework has been designed to address health monitoring challenges through an efficient spectrum system. The primary objective of the design is to allocate individual radio spectrum channels for seamless communication, a factor particularly vital during the COVID-19 pandemic for patient monitoring through the IoMT framework. The author emphasizes channel allocation to prevent packet loss and ensure effective resource utilization [28].

B. Thermal-image based skin temperature screening

In [29], researchers developed a real-time alert notification system by tracking objects exhibiting abnormal fever symptoms and assigning them an identification tag for continuous recognition. In [30], the authors employed infrared thermography (IRT) to detect various symptoms during early stages. They utilized a Convolutional Neural Network (CNN) model to detect and classify cancers, incorporating features such as dry eye syndromes and skin temperatures through the skip symptoms feature. Researchers developed a method based on thermal imaging to screen skin temperature, as represented in [31]. They utilized calibrated, error-free thermal devices to minimize noisy and redundant data [32] while measuring temperatures across different facial areas. In [33], [34], a novel stress detection method has been developed to classify stressed individuals based on both skin temperature and physiological characteristics. The study achieved notable results by analysing various features extracted from thermal data, and they tested the model in applications for real-time performance analysis. In [35], the author developed a Region of Interest (ROI) method based on four views of features extracted from thermal images using the Fast Fourier Transform (FFT) power spectrum. From this study, we inspired to design a lightweight model as an initial step to classify objects; the defective skin temperature object is taken to process the next steps; otherwise, check the objects until the downfall threshold value of the skin temperature. Body temperature measurements are recorded as video, which is to be used to classify and process further steps in our proposed mechanism described in bellow sections.

III. Proposed model

This section outlines the proposed identification and monitoring system that enable DNN structure and cloud computing framework. The system process is divided into multiple segments as per their working principle, and it utilizes three different data sets: real-time sensor data, optical/thermal image data, and medical laboratory history data (optional) as illustrated in Fig. 1. HWSs like heart rate sensor, an ECG sensor, a respiration rate sensor, and a blood-oxygen level

This article has been accepted for publication in IEEE Journal of Biomedical and Health Informatics. This is the author's version which has not been fully edited and content may change prior to final publication. Citation information: DOI 10.1109/JBHI.2024.3400878

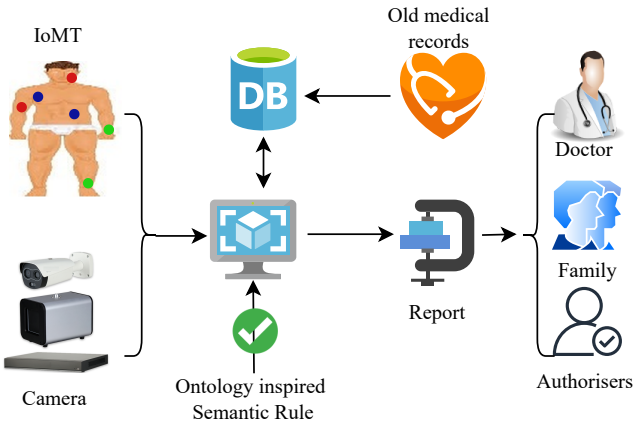

Fig. 1: AWS-inspired disease screening framework

sensor are used to collect the real-time data. The *thermal measurement system* measure the skin temperature of facial entities (forehead, ears, etc.) based on infrared rays to determine the thermal range. Generally, body and facial temperatures are relatively uniform, ranging from 35.5°C to 37.5°C. The *edge processing image system* identify and analyse sensory data as well as lip color using normal images. This process begins when the respiration rate and skin temperature show an abnormal condition. Moreover, the system will identify the lung nodules based on color, size, and breath count features using the data from an ultrasound scanner and is preferred during abnormal conditions of respiration and heart rate. The HWSs stream data to the cloud/fog server through mobile gateways for distinct computation processes, and the combined data is securely stored in the database repository (refer our recent article [36] for more information). Further our system is equipped with three models: Heap correlation rate (HCQ), probability probability least weight square (PPLWS) method, and Data Normalization (DN) factors. These models are evaluated to determine their effectiveness in predicting the status of C-19 and SARS. The following steps helps understand the functionality of our system.

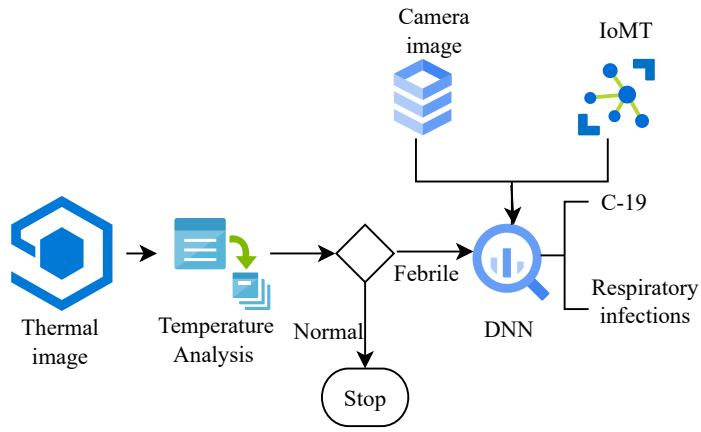

Fig. 2: Deep-learning inspired C-19 prediction model

1) *Data Fusion*: In this step, the Jetson device processes the image and sensor data collected from sensors. As a result, a correlation matrix is constructed based on time-series to prevent data loss during abnormal conditions. A detailed description is provided in the following sections.
2) *Variation Encoder*: In this step, the layer weights, feature weights, and correlation quotient factors under the thermal image-based skin temperature encoder play crucial roles in accurately assessing variations in RoIs (Regions of Interest).
3) *Computing analysis*: In this step, we are evaluating the Heap Correlation Quotient (HCQ), the Prognosticate Probabilistic Least Weight Square (PPLWS) method, and the Data Normalization (DN) factor to cross-verify the predicted results.
4) The *policy of semantic rules inspired by ontology*: In this step, we associate these rules with positive symptoms and further discuss them in the following subsections. Please note that these diet plan suggestions apply only if the symptoms range is close to being positive.

A. Data collection and pre-process

Generally, two types of sensors are used in the data fusion section: medical data and data sensed based on the objectives listed above. The data is stored in matrix representation to improve efficiency and facilitate further computation and analysis in the data collection section. Unlabeled data are considered to assess risk estimates and eliminate factors to make accurate decisions. Medical report records including blood pressure, oxygen level, and measurement index values are used in prediction of COVID-19. In many cases, mixed data may have different dimensions. Therefore, we used filtering techniques to avoid false decisions in below subsection.

1) Missing-data filtering: Most IoMT devices generate redundant data in time-series, and damaged devices will produce noisy data that potentially leads to incorrect decision-making. Likewise, an essential information within the collected data may become obscured during the mining process while estimating semantic features. So, we employed an unlabeled filter to eliminate noise, repetitive records, and irrelevant data according to their maximum variance rate. Subsequently, the following filter restores the lost data by calculating the mean values from the available data, as shown in below Eq. 1.

$$\overline{F^{X_j}} = \frac{1}{2N} \sum_{i=1}^{F} F^{X_j} \tag{1}$$

Here, $\overline{F^{X_j}}$ represents the mean value of the characteristics of the data associated with the pattern cluster X_j for the j^{th} patient. $\overline{F^{X_j}}$ denotes the feature value of the sensed data for the j^{th} patient in the sample pattern cluster X_j. N represents the total number of samples. F Indicates the number of features in the sensed data. These values are substituted when dealing with data loss related to the correlation coefficient between the detected data and medical data.

2) Ontology inspired semantic rule policy: Our proposed system includes the Ontology-inspired semantic rule policy, which facilitates the integration of facts and semantic rules.

This article has been accepted for publication in IEEE Journal of Biomedical and Health Informatics. This is the author's version which has not been fully edited and content may change prior to final publication. Citation information: DOI 10.1109/JBHI.2024.3400878

These facts typically include symptoms and medical data features. Semantic rules encompass both predicted outcomes and the health condition of the patient. We consider 25 rules that map the diet plans of patients to improve their immune system. The use of these rules is formulated using the equations 2 and 3 below.

$$\begin{aligned}&\text{Patient}(\text{F}_i) \cap \text{BMI}(\text{F}_i, \text{no}) \cap \text{HR}(\text{F}_i, \text{abnormal}) \cap \\ &\text{Temp}(\text{F}_i, \text{abnormal}) \cap \text{Re}spi(\text{F}_i, \text{normal}) \cap \\ &\cap \text{Exercise}(\text{F}_i, \text{NO}) \cap \ldots \cap \rightarrow \text{Re}c(\text{F}_i, \text{Diet food})\end{aligned} \tag{2}$$

$$\begin{aligned}&\text{Patient}(\text{F}_i) \cap \text{BMI}(\text{F}_i, \text{high}) \cap \text{HR}(\text{F}_i, \text{normal}) \\ &\cap \text{Exercise}(\text{F}_i, \text{NO}) \cap \ldots \cap \rightarrow \\ &\text{Re}c(\text{F}_i, \text{Phy}_{\text{Activity}})\end{aligned} \tag{3}$$

Note: For detailed understanding please check Appendix.

B. C-19 Deep-learning framework

Image segmentation and ROI are two essential factors in our framework. Figure 2 illustrates the functional flow of our proposed framework. We employed YOLO (You Only Look Once) [37] for Region of Interest (ROI) analysis in the context of fever screening, followed by using a Variance Encoder (VEN) to assess the difference in ROI. We know YOLO is a real-time object detection system that identify and locate objects within an image or video frame. Note that the optical image analysis will be takes place when the skin temperature and IoT device data are abnormal.

1) Thermal-image based cross-validation architecture: This subsection outlines thermal image-based c-19 classification architecture. During the thermal data collection, we preferred detecting skin temperature outdoors because thermal measurements show a slight variation when taken indoors as opposed to outdoors. In our approach, we used the combination of two different thermal and an optical camera data. Figure [**?**] illustrates that if skin temperature readings are abnormal, the process continues to check optical data and real-time wearable sensor data to classify affected individuals in crowded areas, and the AWS-based alert notification system notifies respective authorities. This system also facilitates a tracking service that screens the hospital test reports to strengthen remote diagnosis effectively and reliably. The general measurement of human body temperature is 37°C (98.6°F), but the abnormal facial temperature can vary from person to person, especially when wearing a face mask. Therefore, we trained Region of Interest model to detect the forehead temperature on the face. In our two-step design, the assessment of skin temperature is not the final decision as can see in algorithm 1 that assesses the video to find the abnormal individuals. Figure 3 illustrates the skin temperature analysis based on thermal images. In the context of regions of interest (RoI) analysis, YOLO identifies ROI and assign bounding box for effective tracking. YOLO's real-time processing capability and high accuracy make it a valuable option for monitoring and analyzing RoIs, such as tracking individuals with fever symptoms in crowded areas. A variance encoder (VEN) is proposed based on statistical techniques to assess the differences in RoI, particularly in the context of fever screening. VEN helps analyze data variance from various RoIs, like temperature measurements at different screening locations. It offers a way to examine how the RoIs differ and whether these differences are statistically significant. As the author knowledge the VEN architecture is a robust method for evaluating the effectiveness of fever screening strategies and identifying areas or groups that may require adjustments for better RoI detection and control. Most existing

Algorithm 1: Skin temperature analysis

input : Features F=$f^1, f^2, , f^F ofC-19$
output: Febrile list

```
Let initialize η̂[k] ≠ 0 # thermal image data frames,
  Γ ≠ 0 # clip length in frames;
while Γ ≠ 0 do
    for each η̂[k]inK do
        η̂[k] ← update 3 thermal frames per second;
        # Measure RoI, i.e ℝ;
        ℝ(k) ← YoLo(η̂[k]);
        # Febrile list, i.e 𝔸 with VEN: Variance
          Encoder;
        𝔸(k) ← VEN(ℝ(k), η̂[k]);
    end
end
```

models focus on normalizing the weights of features that led abnormal Mean Squared Error (MSE) rate, resulting in reduced accuracy. Unlike the existing methods, it is essential to forecast the weight of each class and classify them to trace the optimal solution with the DRL architecture backbone. The matrix representations of specific feature weighting are based on Eq. 4.

$$\begin{pmatrix} \varpi_{11} & \varpi_{12} & \varpi_{13} \\ \varpi_{21} & \varpi_{22} & \varpi_{23} \\ \varpi_{31} & \varpi_{32} & \varpi_{33} \end{pmatrix} \tag{4}$$

The particular weight is calculated with Eq. 5.

$$\varpi_{ij} = \frac{1}{N} \sum_{j=1}^{m} \sum_{\text{K}}^{n} X\left(K|f_j\right) \times \sqrt{\frac{X\left(K|f_j\right)}{X\left(K\right)}} \tag{5}$$

Where K and ϖ_{ij} refer to the feature value of the class and the specific feature weight rate f_j of class X, respectively. The value of ϖ_{ij} is associated with the feature state f_j, where a distinct weight indicates an assigned feature state. ϖ_{ij} remains between 0 and 1, representing the crucial feature value for f_j in the C-19 identification. The primary purpose of obtaining these feature weights is to use them as initial weights in the DNN model to enhance predictive results. In this task, classifications are performed with prediction models. The ROI results further cross-validated to avoid incorrect skin temperature detection's due to face-masks and beards.

2) HCQ method: The Heap Correlation Quotient (HCQ) method estimates the association matrix of cluster patterns based on patient variations with notable feature coordinates, such as a and b. The proportion rate is determined using Equation 7 for the range $-1 \leq \Phi_a^b \leq 1$. This calculation follows the condition described in Equation 6.

$$\Phi_a^b = \begin{cases} < 0, \text{ Negative correlation;} \\ = 0, \text{ No correlation and independent;} \\ > 0, \text{ Positive correlation;} \end{cases} \tag{6}$$

This article has been accepted for publication in IEEE Journal of Biomedical and Health Informatics. This is the author's version which has not been fully edited and content may change prior to final publication. Citation information: DOI 10.1109/JBHI.2024.3400878

$$\Phi_a^b = \frac{1}{N} \times \sqrt{\frac{a_i \cdot b_i - \gamma_i \cdot \overline{(a_i b_i)}}{\gamma_i \cdot \widehat{a}_i \cdot \widehat{b}_i}} \tag{7}$$

Where N refers to cluster patterns, a_i and b_i are respective cluster patterns (CP_i), $\overline{(a_i b_i)}$ refers to the product mean of a_i and b_i, and $\widehat{a}_i$, $\widehat{b}_i$ refer to the standard deviations of a_i and b_i.

3) Data-Normalization: The sensory measured dataset includes various features with nonidentical numerical values that causes increasing computational complexity. To address this issue, a HR-Normalization is employed to normalize the sensed values with a range [0,1], as described in Equation 8.

$$DN = \frac{1}{N \cdot \mathrm{X_{Hig}} \cdot \mathrm{X_{Lea}}} \times \sqrt{\left(\frac{\mathrm{X_{SD}} - \mathrm{X_{Lea}}}{\mathrm{X_{Hig}} - \mathrm{X_{Lea}}}\right)} \times \left(\hat{\mathrm{X}}_{\mathrm{Hig}} - \hat{\mathrm{X}}_{\mathrm{Lea}}\right) + \hat{\mathrm{X}}_{\mathrm{Lea}} \tag{8}$$

Where DN represents a normalized value calculated using the source sensed or medical data (X_{SD}), where the most negligible data value denotes X_{Lea}, and the highest data value (X_{Hig}). It is computed as a function involving the square root and the converted dataset range represented by $\hat{\mathrm{X}}$Lea and $\hat{\mathrm{X}}$Hig. The preferred values for $\hat{\mathrm{X}}$Lea and $\hat{\mathrm{X}}$Hig are 0 and 1 respectively, that ensures the bounded range $[0, 1]$.

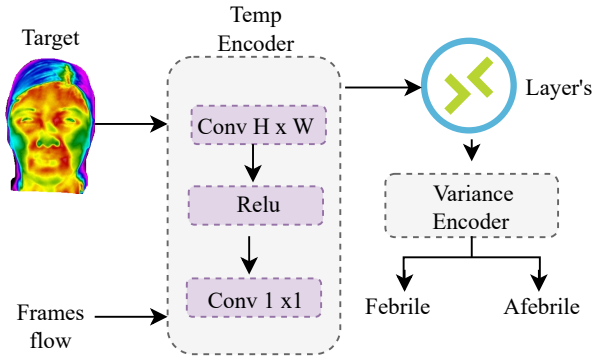

Fig. 3: Skin temperature analyses

4) PPLWS model: The Prognosticated Probabilistic Least Weight Square (PPLWS) and HCQ models are designed based on DNN architecture, as shown in Fig. 2. This mechanism assesses the backpropagation strategies, and the inclination algorithm for binary analysis of COVID-19. Initially, we considered various features to train the model. The DNN model enable 5 layers (1 input layer + 3 hidden layers + 1 output layer). The input layer contains 32 nodes, as indicated by the feature numbers of the dataset. It is essential to determine the number of nodes in the hidden layers on the basis of the neural model, i.e 25 nodes with fully connected layers. Credits are assigned to the DNN model through the input layer, and these assignments are passed to the three hidden layers by adjusting their respective weights. The overall weight is calculated and bias is included to process the information by the hidden layer nodes, as shown in Eq. 9.

$$\phi_j = \frac{1}{F} \sum_{i=1}^{F} \sum_{j=1}^{m} a_i \times \varpi_{ij} \times \Theta_j \tag{9}$$

Where a_i, ϖ_{ij}, and Θ_j describe input data, the weight among devices, and the bias value, respectively. The changed information is fed into the output layer to predict the presence or absence of C-19. The output layer comprises two devices that provide binary predictions (C-19 absence and C-19 presence). Initially, the DNN-PPLWS system starts with various initial weights based on sensed and medical sources. Subsequently, the differential error rate between real-time embedded systems and expected medical output remains limited due to the backpropagation mechanism. When training the DNN model, the weights are updated using Eq. 10.

$$\psi_{ij} = 1 - \gamma \times \frac{1}{\varpi_{ij}} \times \frac{d}{dx}(\Upsilon) \tag{10}$$

Where γ describes the rate of learning, declared constant, and Υ signifies error, which is determined by Eq. 11.

$$\Upsilon_j = 0.75 \times \sum_{s=1}^{S} \sum_{r=1}^{R} \sqrt{(\mathrm{P} - Q)^2} \tag{11}$$

Where S and R denote the number of instances and outputs, and P, Q denotes the suitable output and the actual output, respectively. Training error plays a vital role in adjusting all weights and then reevaluates the predictions of the output layer. The procedure is repeated until the system achieves a minimal error between the actual output and the predicted output. Therefore, the approximate DNN rate remains at 0.04. The Adam approach [38] enhances the DNN model, the respective steps reflected in algorithm 2.

IV. Experimental Results

In this section, we present the simulation results of our proposed C-19 system, conducted in MATLAB R2021 on a Lenovo PC with an Intel(R) Core i5-2557M 1.70GHz processor and 16GB RAM. The COVID-19 Open Research dataset (CORD-19) and FAB-lab datasets were utilized for performance assessment. We employed the Thingspeck plugin [39] for sensor data visualization, where an external key shareable for monitoring measured values through the link https://thingspeak.com/apps/plugins/178859. Prediction models, including Logistic Regression, eXtreme Gradient Boosting (XGBoost), Multi-layer Perceptron (MLP), and Support Vector Machine (SVM), were implemented using the Waikato Environment for Knowledge Analysis (Weka) software. The evaluation of model performance involved metrics such as accuracy, precision, sensitivity, and specificity to identify the optimal model for COVID-19 prediction.

Numerical data were collected using Human Wearable Sensors (HWSs) for measuring oxygen levels, thermal temperature, and respiration rate. Data computations for accurate predictions regarding the presence or absence of COVID-19 are performed using a high-capacity microcontroller. Simulations are conducted with two different datasets: Covid-19 USA data released by the New York Times [40] and thermal image data + clinical data [41]. The performance analysis across different models using three distinct datasets—Covid-19 NYT, thermal data, and CORD-19 presented in Tables I, II, and III, respectively. Each table provides insights into the precision, F-score,

This article has been accepted for publication in IEEE Journal of Biomedical and Health Informatics. This is the author's version which has not been fully edited and content may change prior to final publication. Citation information: DOI 10.1109/JBHI.2024.3400878

Algorithm 2: C-19 prediction

input : Features F=$f^1, f^2, , f^F ofC-19$
output: C-19 identification

Let initialize $\varpi_{ij}=0$, $\Theta_j=0.125$, $\Upsilon_j=0$, $\gamma=0.04$;
while $f^i \neq 0$ **do**
  for *each* $f_i \in f_N$ **do**
    Estimate the weighted sum of each hidden layer using Eq. $\phi_j = \frac{1}{F}\sum_{i=1}^{F}\sum_{j=1}^{m} a_i \times \varpi_{ij} \times \Theta_j$
    for $each j \in m$ **do**
      $\psi_{ij} = 1-\gamma \times \frac{1}{\varpi_{ij}} \times \frac{d}{dx}(\Upsilon)$;
      Estimate the error rate of each instance I using Eq.

$$\Upsilon_j = 0.75 \times \sum_{s=1}^{S}\sum_{r=1}^{R}\sqrt{(\mathrm{P}-Q)^2}$$

      Update feature weighting matrix using Eq. 4;
      if $\Upsilon_j \leq$ *threshold* **then**
        Update matrix set;
        f(I)=max(0,ψ_{ij}) to estimate the C-19 instance I;
      end
      else
        Continue testing and monitoring until error becomes minimal between P and Q;
      end
    end
  end
end

and recall metrics for both training and testing phases, offering a comprehensive overview of the model evaluations. In the Covid-19 NYT dataset I, models such as Linear Regression, Random Forest (RF), Support Vector Machine (SVM), Naive Bayes, VEN+RF, VEN+SVM, and VEN+NB are assessed. The variations in performance metrics between training and testing phases are observed, highlighting the models' abilities to generalize the prediction results, and similar for other two datasets. In average, the VEN+RF model shows robust performance across datasets, with notable precision, F-score, and recall values during both training and testing phases. Its ability to harness the strengths of Random Forest (RF) enhances predictive accuracy. VEN+SVM showcases high precision and recall, indicating strong predictive capabilities, while maintaining consistency between training and testing results. VEN+NB demonstrates impressive precision and recall, underscoring its efficacy in capturing patterns within datasets. These ensemble models, combining Variational Autoencoder Network (VEN) with established algorithms, offer promising results for diverse applications, showcasing their adaptability and effectiveness in predictive modeling tasks.

The datasets divided into 75% and 25% for better performance analysis. Initially, we converted medical report data and

TABLE I: Performance analysis using Covid-19 NYT

Model	Precision		F-score		Recall	
	training	testing	training	testing	training	testing
Liner regression	0.669	0.515	0.741	0.593	0.809	0.635
RF	0.897	0.860	0.745	0.718	0.641	0.620
SVM	0.823	0.767	0.697	0.451	0.616	0.481
Naive Bayes	0.642	0.981	0.987	0.799	0.989	0.792
VEN+RF	0.813	0.931	0.670	0.699	0.546	0.678
VEN+SVM	0.9777	0.781	0.813	0.627	0.873	0.820
VEN+NB	0.985	0.799	0.989	0.789	0.980	0.781

TABLE II: Performance analysis using thermal data

Model	Precision		F-score		Recall	
	training	testing	training	testing	training	testing
Liner regression	0.791	0.834	0.914	0.856	0.897	0.892
RF	0.892	0.913	0.948	0.9392	0.978	0.951
SVM	0.850	0.868	0.923	0.966	0.972	0.977
Naive Bayes	0.890	0.928	0.938	0.943	0.980	0.989
VEN+RF	0.956	0.961	0.880	0.870	0.791	0.812
VEN+SVM	0.922	0.919	0.930	0.914	0.931	0.900
VEN+NB	0.960	0.955	0.886	0.892	0.841	0.836

sensor data into a labeled format. Furthermore, COVID-19 Open Research Dataset Challenge (CORD-19) dataset is used performance analysis. We compare the performance of our model with/without benchmark systems such as Support Vector Machine (SVM), the Naive Bayes classifier, and Decision Tree (DT). We deploy our proposed model before and after feature selection and analyze the results as shown in Figures 5 to 6 below.

Fig. 5(a) illustrates data fusion accuracy collected in two ways: from sensors and a medical lab. The collected data include 10 to 13 characteristics and SVM, DT, and Naive Bayes (NB) classification model performance are measured. Sensor data have a precision of 69%, while medical data have a precision of 68. 75% under the NB model, but it is less accurate due to features limitations. Subsequently, we observed that our model has an accuracy of 73.45% with

TABLE III: Performance analysis using CORD-19

Model	Precision		F-score		Recall	
	training	testing	training	testing	training	testing
Liner regression	0.881	0.875	0.819	0.832	0.885	0.859
RF	0.921	0.893	0.855	0.890	0.823	0.841
SVM	0.963	0.950	0.973	0.830	0.929	0.907
Naive Bayes	0.919	0.884	0.902	0.879	0.964	0.923
VEN+RF	0.952	0.921	0.907	0.881	0.892	0.867
VEN+SVM	0.960	0.936	0.944	0.931	0.930	0.912
VEN+NB	0.984	0.884	0.973	0.846	0.967	0.945

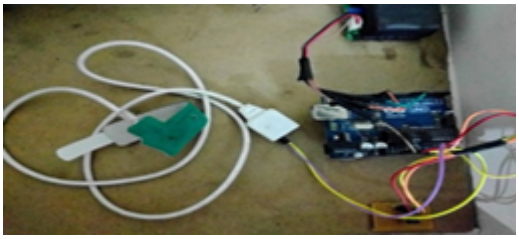

Fig. 4: IoMT setup

This article has been accepted for publication in IEEE Journal of Biomedical and Health Informatics. This is the author's version which has not been fully edited and content may change prior to final publication. Citation information: DOI 10.1109/JBHI.2024.3400878

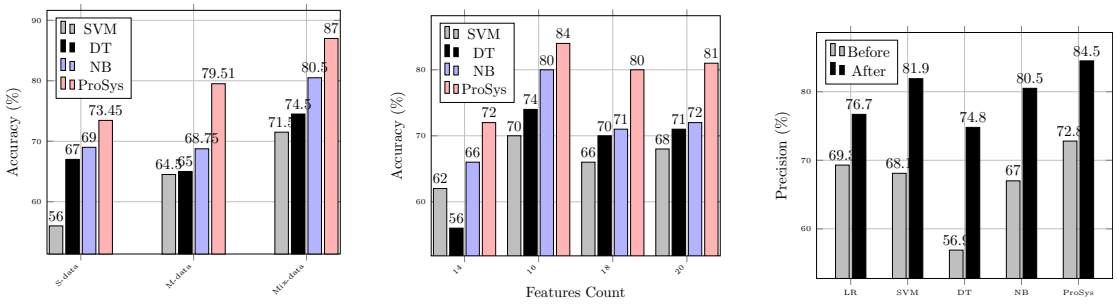

(a) Data fusion accuracy analysis (b) Feature count based accuracy analysis (c) Precision Analysis

Fig. 5: Data fusion accuracy analysis of LAB data

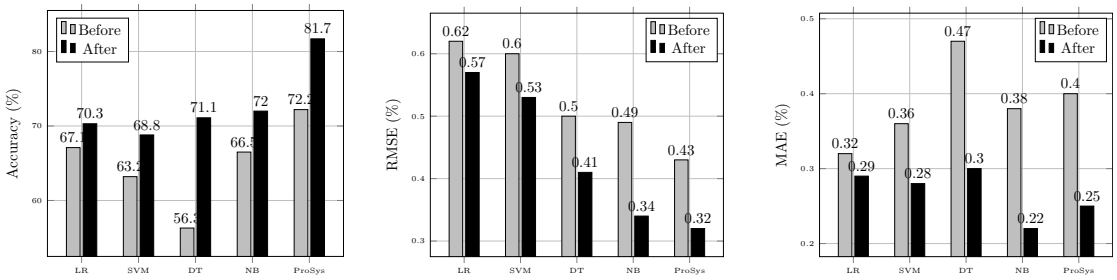

(a) Accuracy analysis (b) RMSE analysis (c) MAE Analysis

Fig. 6: Data fusion accuracy analysis of before and after proposed method on LAB dataset

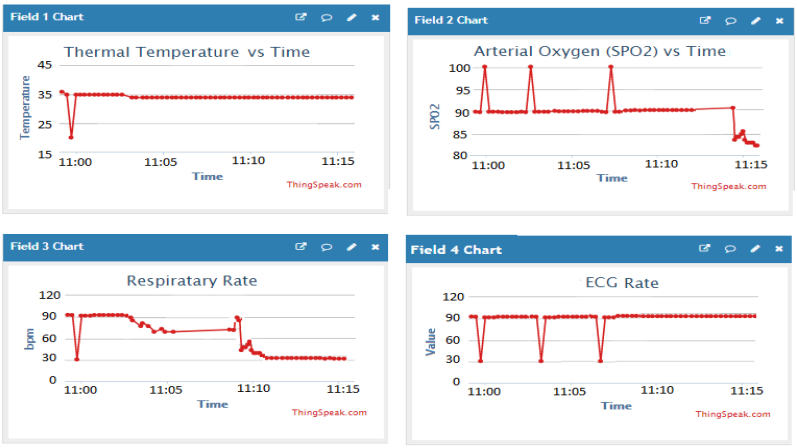

Fig. 7: Real-time sensor data visualization

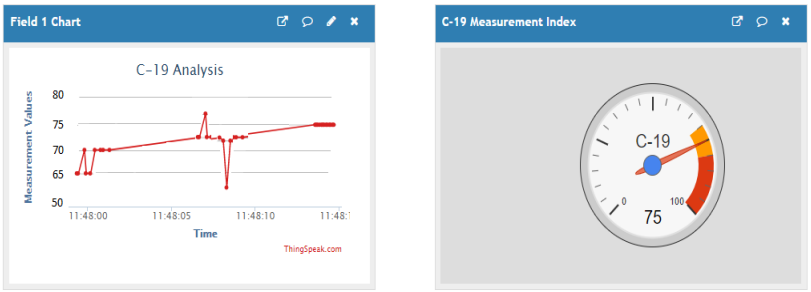

Fig. 8: C-19 measurement analysis

This article has been accepted for publication in IEEE Journal of Biomedical and Health Informatics. This is the author's version which has not been fully edited and content may change prior to final publication. Citation information: DOI 10.1109/JBHI.2024.3400878

TABLE IV: Performance analysis using FEB lab data

Model	16 features		20 features		Recall		F-score	
	training	testing	training	testing	training	testing	training	testing
Liner regression	0.698	0.679	0.703	0.697	0.695	0.675	0.688	0.672
RF	0.684	0.690	0.612	0.609	0.689	0.672	0.691	0.680
SVM	0.708	0.712	0.685	0.668	0.691	0.683	0.657	0.663
DT	0.742	0.726	0.717	0.700	0.705	0.699	0.680	0.664
Naive Bayes	0.805	0.781	0.726	0.719	0.712	0.706	0.693	0.689
VEN+NB	0.841	0.828	0.819	0.802	0.836	0.815	0.827	0.810

sensor data, 79. 51% with medical data and 87% with mixed data compared to other models. The simulation results show that our system achieved a notable C-19 identification rate with different features count compared to other models.

Feature-based training influence the performance of the system and are mutually dependent on each other. We conducted simulations with various count of features, including 16 and 20 features. Fig. 5(b) illustrates the classifier accuracy based on the selected feature sets, and Fig. 5(c) shows the analysis of the precision ratio. Observe that all models have a lower accuracy rate when 16 features. The feature selection analysis shown in Figure 6 with four metrics: precision, precision, MAE (mean absolute error) and RMSE (radio mean square error). Multiple features are evaluated on the basis of our designed probability models. Additionally, we simulate a fuzzy analytical hierarchy process and PPLWS to estimate the performance. Our model achieves significantly higher accuracy compared to the remaining models due to Heap Correlation Quotient (HCQ) feature selection approach. The MAE and RMSE also have lower error rate that can be observe in Figures 6(a) to 6(c).

A. Thingspeck Result Analysis

Fig. 7 illustrates wearable sensor setup connected with microcontroller for computation and visualization on the Thingspeck. The external key is shareable with physicians and hospitals for remote monitoring using phones or the Thingspeck. Thingspeck offers services with channels for accurate control and monitoring. As we are aware of the importance of SpO_2 levels in the blood, it is crucial to note that temperature, SpO_2, and bpm are independent factors used to assess the importance of monitoring the patient condition.

Fig. 8 shows the values of the C-19 measurement index. The designed index assesses the priority situation and generates instructions for assessing the continuation phase of the C-19 tests. The gauge meter refers to the C-19 phases, where the yellow indicates the need for vigilant monitoring, and the red indicates the need for next-level tests and the primary suspicion of the C-19 virus. In the next phase, lip color and lung functioning assessed to make precise decision using the equation below (Eq. 12).

$$\varphi(f_i) = \log_{10}(2) \times \left(\eta_i + \varepsilon_i + \omega \cdot \vartheta_{10}^i\right) \tag{12}$$

Where ϑ_{10}^i, η_i, ε_i, and $\omega = 1.005$ refer to the temperature quotient, oxygen saturation rate, respiration rate, and constant weight, respectively.

$$\vartheta_{10}^i = \left(\frac{\alpha_1}{\alpha_2}\right)^{\left(\frac{10^\circ C}{T2-T_1}\right)} \tag{13}$$

Where α_1 and T_1 refer to the temperature rate and thermal temperature, respectively.

TABLE V: Device specifications

Device	Normal	Thermal
Model	Medvision GigE	Fortic 680
Data type	Visible	Infrared
Resolution	640x480	640x480
FPS	25∼30	25∼30
Coverage degree	90	90

B. Thermal image processing importance

For effective evaluation as we have considered multi-modality data to screen the virus symptoms. Table V outlines the camera specifications which is used record where two cameras are used like thermal and normal camera. Like if the temperature is abnormal, the corresponding normal image is considered to assess the lip color (this feature helps in classifying lip colors) and face expressions.

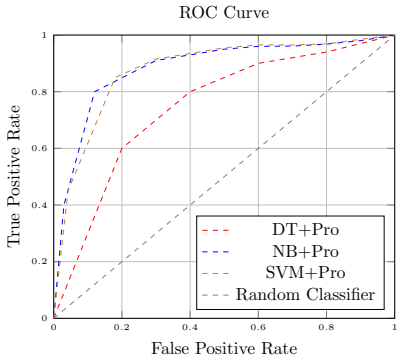

(a)

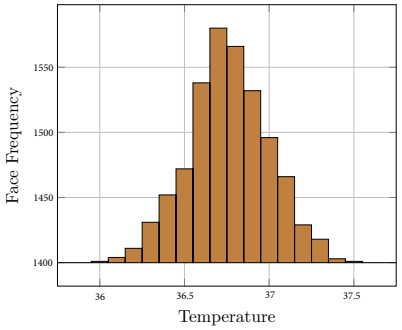

(b)

Fig. 9: ROC curve and face frequency analysis

Figure 9 illustrates the performance of the proposed model after cleaning the dataset and combining all the features extracted from multimodal data. We used machine learning base learners to assess the model's classification accuracy. Naive Bayes, as observed in Figure 9(a), achieved notable

TABLE VI: Comparison results. TRAC is training accuracy, TEAC is testing accuracy, TRL is training loss, TEL is testing loss

Metrics	VGG19	ResNet50	DensNet21	Xception	VEN+YoLo
ROC	93.12	90.20	94.69	93.98	95.23
Precision	93.32	89.53	93.91	92.47	94.59
TRAC	93.09	88.10	94.01	92.65	95.06
TRL	0.16	0.32	0.09	0.21	0.06
TEAC	93.12	88.90	94.23	92.98	95.34
TEL	0.15	0.30	0.13	0.20	0.12

accuracy, surpassing SVM and DT. Similarly, skin temperature is the primary feature influencing the decision to proceed or not. Figure 9(b) illustrates the frequency ratio of the face with the measured temperature, showing that, on average, the temperature remains normal in most time series frames. Table VI presents the simulation results with state-of-the-art (SOTA) models. Our (VEN+YoLo) model has achieved remarkable results, including a 95.23% ROC, a 94.59% precision, a 95.06% training accuracy, a 0.06% training loss, a 95.34% testing accuracy and a 0.12% testing loss.

V. Conclusion

This paper introduces an innovative C-19 screening and monitoring system aimed at addressing remote diagnosis challenges through a deep learning-inspired data fusion model. The Variation Encoder (VEN) accurately evaluates skin temperature using Regions of Interest (RoI) identified by YoLo. The data fusion model integrates features extracted from electronic records and sensor data from wearable human sensors. Employing a data accumulation method, unnecessary features are eliminated, reducing computational load and enhancing performance rates to 47% and 91%, respectively.

Furthermore, a contingent probability method estimates distinct feature weights for each cluster, improving performance by eliminating anomalous data. Simulation results showcase outstanding performance with a data accuracy of 95.2%, surpassing traditional techniques like kernel random forest, correlation-based feature selection, sequential forward selection, and wavelet transformation.

Appendix

Based on the patient's routine habits, including the regular medication they receive, we fed this information into the model to generate dietary rules aimed at improving the patient's immune system. We have considered two case studies as follows in the remote screening-monitoring context.

Corollary 1. *We have established a set of conditions and actions involving patient attributes (F_i) and various health-related factors. These conditions are integral to our smart system that makes informed decisions about patient care and treatment plans. This set of rules allows our system to identify patients who may need specific interventions, such as dietary changes or increased physical activity, based on their individual health profiles.*

As defined in Equation 2, each component has a specific role: Patient(F_i) represents the attributes of the patient, denoted F_i. BMI(F_i) pertains to the Body Mass Index (BMI) attribute and specifies that it is "no," which typically indicates a normal or healthy BMI. HR$(F_i, abnormal)$ involves the Heart Rate (HR) attribute and indicates that it is "abnormal," suggesting an irregular or unhealthy heart rate. Temp$(F_i, abnormal)$ refers to the Temperature attribute and states that it is "abnormal," possibly indicating a fever or an unusual body temperature. $\mathrm{Respi}(F_i, normal)$ *is associated with respiratory or pulmonary attributes, potentially related to spirometry, and specifies that it is "normal," indicating typical or healthy respiratory function. Exercise(F_i, NO) checks the patient's exercise habits and indicates "NO," suggesting that the patient does not engage in exercise or physical activity. In conclusion, on the basis of these rules, the suggested course of action is* $\mathrm{Rec}(F_i, Diet\ food)$

References

[1] S. Roy, K. Powell, and L. W. Gerson, "Temporal artery temperature measurements in healthy infants, children, and adolescents," *Clinical pediatrics*, vol. 42, no. 5, pp. 433–437, 2003.

[2] "COVID-19 coronavirus pandemic," 2020. [Online]. Available: https://www.worldometers.info/coronavirus/?utm_campaign=homeAdvegas1

[3] "Using IoT to fight COVID-19 pandemic," 2020. [Online]. Available: https://www.eetasia.com/using-iot-to-fight-covid-19-pandemic/

[4] A. Wilson, K. Gupta, B. H. Koduru, A. Kumar, A. Jha, and L. R. Cenkeramaddi, "Recent advances in thermal imaging and its applications using machine learning: A review," *IEEE Sensors Journal*, 2023.

[5] A. Barnawi, P. Chhikara, R. Tekchandani, N. Kumar, and B. Alzahrani, "Artificial intelligence-enabled internet of things-based system for covid-19 screening using aerial thermal imaging," *Future Generation Computer Systems*, vol. 124, pp. 119–132, 2021.

[6] M. I. Uddin, S. A. A. Shah, and M. A. Al-Khasawneh, "A novel deep convolutional neural network model to monitor people following guidelines to avoid covid-19," *Journal of Sensors*, vol. 2020, pp. 1–15, 2020.

[7] N. D. Kathamuthu, S. Subramaniam, Q. H. Le, S. Muthusamy, H. Panchal, S. C. M. Sundararajan, A. J. Alrubaie, and M. M. A. Zahra, "A deep transfer learning-based convolution neural network model for covid-19 detection using computed tomography scan images for medical applications," *Advances in Engineering Software*, vol. 175, p. 103317, 2023.

[8] J. Zhang, Q. Yan, X. Zhu, and K. Yu, "Smart industrial iot empowered crowd sensing for safety monitoring in coal mine," *Digital Communications and Networks*, vol. 9, no. 2, pp. 296–305, 2023.

[9] Z. Shen, F. Ding, Y. Yao, A. Bhardwaj, Z. Guo, and K. Yu, "A privacy-preserving social computing framework for health management using federated learning," *IEEE Transactions on Computational Social Systems*, vol. 10, no. 4, pp. 1666–1678, 2023.

[10] S. Swayamsiddha and C. Mohanty, "Application of cognitive Internet of Medical Things for COVID-19 pandemic," *Journal of diabetes and metabolic syndrome*, vol. 14, no. 5, pp. 911–915, 2020.

[11] N. Zheng, S. Du, J. Wang, H. Zhang, W. Cui, Z. Kang, T. Yang, B. Lou, Y. Chi, H. Long, M. Ma, Q. Yuan, S. Zhang, D. Zhang, F. Ye, and J. Xin, "Predicting COVID-19 in China using hybrid AI model," *IEEE Transactions on Cybernetics*, vol. 50, no. 7, pp. 911–915, 2020.

[12] R. P. Singh, M. Javaid, A. Haleem, R. Vaishya, and S. Ali, "Internet of medical things (iomt) for orthopaedic in covid-19 pandemic: Roles, challenges, and applications," *Journal of clinical orthopaedics and trauma*, vol. 11, no. 4, pp. 713–717, 2020.

[13] T. Yang, M. Gentile, C.-F. Shen, and C.-M. Cheng, "Combining point-of-care diagnostics and internet of medical things (iomt) to combat the covid-19 pandemic," p. 224, 2020.

[14] M. Tsikala Vafea, E. Atalla, J. Georgakas, F. Shehadeh, E. K. Mylona, M. Kalligeros, and E. Mylonakis, "Emerging technologies for use in the study, diagnosis, and treatment of patients with covid-19," *Cellular and molecular bioengineering*, vol. 13, pp. 249–257, 2020.

[15] F. Shi, J. Wang, J. Shi, Z. Wu, Q. Wang, Z. Tang, K. He, Y. Shi, and D. Shen, "Review of artificial intelligence techniques in imaging data acquisition, segmentation, and diagnosis for covid-19," *IEEE reviews in biomedical engineering*, vol. 14, pp. 4–15, 2020.

[16] L. Wynants, B. Van Calster, G. S. Collins, R. D. Riley, G. Heinze, E. Schuit, E. Albu, B. Arshi, V. Bellou, M. M. Bonten *et al.*, "Prediction models for diagnosis and prognosis of covid-19: systematic review and critical appraisal," *bmj*, vol. 369, 2020.

[17] S. Kadry, V. Rajinikanth, S. Rho, N. S. M. Raja, V. S. Rao, and K. P. Thanaraj, "Development of a machine-learning system to classify lung ct scan images into normal/covid-19 class," *arXiv preprint arXiv:2004.13122*, 2020.

[18] Q. He, Z. Feng, H. Fang, X. Wang, L. Zhao, Y. Yao, and K. Yu, "A blockchain-based scheme for secure data offloading in healthcare with deep reinforcement learning," *IEEE/ACM Transactions on Networking*, pp. 1–16, 2023.

[19] X. Yuan, Z. Zhang, C. Feng, Y. Cui, S. Garg, G. Kaddoum, and K. Yu, "A dqn-based frame aggregation and task offloading approach for edge-enabled iomt," *IEEE Transactions on Network Science and Engineering*, vol. 10, no. 3, pp. 1339–1351, 2023.

[20] S. Liu, T. Cai, X. Tang, and C. Wang, "Mrl-net: Multi-scale representation learning network for covid-19 lung ct image segmentation," *IEEE Journal of Biomedical and Health Informatics*, 2023.

[21] K. H. Shibly, S. K. Dey, M. T.-U. Islam, and M. M. Rahman, "Covid faster r–cnn: A novel framework to diagnose novel coronavirus disease (covid-19) in x-ray images," *Informatics in Medicine Unlocked*, vol. 20, p. 100405, 2020.

[22] T. Rahmat, A. Ismail, and S. Aliman, "Chest x-ray image classification using faster r-cnn," *Malaysian Journal of Computing (MJoC)*, vol. 4, no. 1, pp. 225–236, 2019.

[23] R. Sujath, J. M. Chatterjee, and A. E. Hassanien, "A machine learning forecasting model for COVID-19 pandemic in India," *Stochastic Environmental Research and Risk Assessment*, vol. 34, pp. 959–972, 2020.

[24] S. Vaid, R. Kalantar, and M. Bhandari, "Deep learning COVID-19 detection bias: accuracy through artificial intelligence," *International Orthopaedics*, vol. 44, pp. 1539–1542, 2020.

[25] S. Tuli, S. Tuli, R. Tuli, and S. S. Gill, "Predicting the growth and trend of COVID-19 pandemic using machine learning and cloud computing," *Internet of Things*, vol. 11, p. 100222, 2020.

[26] A. M. U. D. Khanday, S. T. Rabani, Q. R. Khan, N. Rouf, and M. M. U. Din, "Machine learning based approaches for detecting COVID-19 using clinical text data," *International Journal of Information Technology*, vol. 12, pp. 731–739, 2020.

[27] M. Muzammal, R. Talat, A. Sodhro, and S. Pirbhulal, "A multi-sensor data fusion en- abled ensemble approach for medical data from body sensor networks," *Information Fusion*, vol. 53, pp. 155–164, 2020.

[28] G. R. Shinde, A. B. Kalamkar, P. N. Mahalle, N. Dey, J. Chaki, and A. E. Hassanien, "Forecasting models for coronavirus disease (covid-19): A survey of the state-of-the-art," *SN Computer Science*, vol. 1, p. 197, 2020.

[29] W. Tan, J. Liu, Y. Zhuo, Q. Yao, X. Chen, W. Wang, R. Liu, and Y. Fu, "Fighting covid-19 with fever screening, face recognition and tracing," in *Journal of Physics: Conference Series*, vol. 1634, no. 1. IOP Publishing, 2020, p. 012085.

[30] M. A. Farooq and P. Corcoran, "Infrared imaging for human thermography and breast tumor classification using thermal images," in *2020 31st Irish Signals and Systems Conference (ISSC)*. IEEE, 2020, pp. 1–6.

[31] H. Metzmacher, D. Wölki, C. Schmidt, J. Frisch, and C. van Treeck, "Real-time human skin temperature analysis using thermal image recognition for thermal comfort assessment," *Energy and Buildings*, vol. 158, pp. 1063–1078, 2018.

[32] D. Li, C. C. Menassa, and V. R. Kamat, "Non-intrusive interpretation of human thermal comfort through analysis of facial infrared thermography," *Energy and Buildings*, vol. 176, pp. 246–261, 2018.

[33] M. Abouelenien, M. Burzo, and R. Mihalcea, "Human acute stress detection via integration of physiological signals and thermal imaging," in *Proceedings of the 9th ACM international conference on pervasive technologies related to assistive environments*, 2016, pp. 1–8.

[34] G. Batchuluun, J. K. Kang, D. T. Nguyen, T. D. Pham, M. Arsalan, and K. R. Park, "Deep learning-based thermal image reconstruction and object detection," *IEEE Access*, vol. 9, pp. 5951–5971, 2020.

[35] F. De Oliveira, S. Moreau, C. Gehin, and A. Dittmar, "Infrared imaging analysis for thermal comfort assessment," in *2007 29th Annual international conference of the IEEE engineering in medicine and biology society*. IEEE, 2007, pp. 3373–3376.

[36] G. Srivastava, M. Mekala, M. S. Hajar, and H. Kalutarage, "C-nest: Cloudlet based privacy preserving multidimensional data stream approach for healthcare electronics," *IEEE Transactions on Consumer Electronics*, 2023.

[37] A. Bochkovskiy, C.-Y. Wang, and H.-Y. M. Liao, "Yolov4: Optimal speed and accuracy of object detection," *arXiv preprint arXiv:2004.10934*, 2020.

[38] M. Z. Alom, T. M. Taha, C. Yakopcic, S. Westberg, P. Sidike, M. S. Nasrin, M. Hasan, B. C. Van Essen, A. A. Awwal, and V. K. Asari, "A state-of-the-art survey on deep learning theory and architectures," *Electronics*, vol. 8, no. 3, p. 292, 2019.

[39] M. A. G. Maureira, D. Oldenhof, and L. Teernstra, "Thingspeak–an api and web service for the internet of things," *World Wide Web*, vol. 25, pp. 1–4, 2011.

[40] "Coronavirus (covid-19) data, united states," 2021. [Online]. Available: [Online].Available:https://github.com/nytimes/covid-19-data

[41] J. Tamez-Peña, A. Yala, S. Cardona, R. Ortiz-Lopez, and V. Trevino, "Upper body thermal images and associated clinical data from a pilot cohort study of covid-19," *PhysioNet, Ed., PhysioNet*, 2021.